GPS Solut (2014) 18:41–50
DOI 10.1007/s10291-012-0307-3

ORIGINAL ARTICLE

Real-time clock jump compensation for precise point positioning

Fei Guo · Xiaohong Zhang

Received: 27 March 2012 / Accepted: 15 December 2012 / Published online: 3 January 2013

Abstract Over the past decades, a number of methods have been proposed to handle cycle slips in the carrier phase measurements, but few researches have investigated receiver clock jumps, which may produce undesirable effects on GPS data processing. Such events are generally ignored in double-differenced positioning. For undifferenced processing, such as precise point positioning (PPP) techniques, it is unwise to neglect the impact of clock jumps. Failure to properly detect and account for receiver clock jumps may sometimes cause unexpected behavior of the GPS software and large errors in the resulting PPP solution. This is particularly troublesome when there are irregular (types 2 or 3) millisecond clock jumps represented in RINEX observation files. In this study, we first provide an intuitive description of the receiver clock jump phenomenon, and a comprehensive classification of clock jumps is presented according to its influence on three fundamental quantities (time tag, pseudorange, and carrier phase) of RINEX observation files. To follow the RINEX convention, the observable consistency is analyzed for various types of clock jump; and a simple but robust real-time clock jump compensation (RTCJC) method is proposed for reconstructing a consistent set of observables. Numerous validation tests with various GPS data show that the method is applicable to millisecond clock jumps. Without RTCJC, clock jumps are prone to cause failure of gross error and cycle slip detection algorithms and so result in repeated re-initialization or even non-convergent solutions, which lead to gross errors in the PPP solution. When RTCJC is applied, all clock jumps present in the GPS data can be effectively identified and repaired accurately, and the problem of re-initialization in PPP will no longer be triggered by receiver clock jumps, which results in significant improvement of PPP accuracy and reliability.

Keywords Precise point positioning · Receiver clock jump · Clock jump detection · Clock jump repair · Real-time clock jump compensation

F. Guo · X. Zhang (✉)
School of Geodesy and Geomatics, Wuhan University,
129 Luoyu Road, Wuhan 430079, People's Republic of China
e-mail: xhzhang@sgg.whu.edu.cn

F. Guo
e-mail: fguo@whu.edu.cn

Introduction

Receivers with cheap internal oscillators like the Ashtech or Trimble receivers attempt to keep the internal clocks of oscillators synchronized with GPS time to prevent the clock bias becoming too large. This is done by periodically clock resets (Kim and Langley 2001; Lonchay et al. 2011). Although the actual mechanism of how the clock in a particular manufacturer's receiver is adjusted varies from one manufacturer to another, two approaches are commonly adopted in this regard. First, the receiver can steer the oscillator to drive the clock bias to approximately zero, in which case the offset is constant to within the level of noise and tracking jitter. Second, and, perhaps, more common, the receiver introduces discrete jumps in the receiver's estimate of time. These jumps typically occur when the clock offset exceeds 1 ms in magnitude and hence are often called "millisecond (ms) jumps." The millisecond jumps are typically jumps by an integer number of milliseconds.

Once a clock jump occurs, three fundamental RINEX quantities (time tag, pseudorange, and carrier phase measurement) are prone to be affected by discontinuities (Kim

and Lee 2009). Due to the clock behavior, the carrier phase and pseudorange observables should both have a sawtooth clock signature; however, only the range observables have the sawtooth. The phase is computed based on the true oscillator, without the offsets introduced by the clock adjustments (Freymueller 2003, IGSMAIL-4318). This phenomenon of inconsistency in GPS raw measurements caused by receiver clock jumps can produce undesirable effects in the data processing stage (Lonchay et al. 2011). To generate a consistent set of observable, GPS tools like TEQC (Estey et al. 1999) and ClockPrep (Freymueller 2003) are currently widely used for reconstruction with different options available. RINEX, as it was presented by Gurtner and Estey (2007), prescribes that we have to reconstruct a consistent set of phase, code, and epoch values when the receiver or the converter software adjusts the measurements using the real-time-derived receiver clock offsets. However, these tools cannot always correctly convert RINEX. Failures in properly detecting and accounting for clock resets can sometimes lead to unexpected behavior of the PPP software and incorrect estimation (Mireault et al. 2008). It is particularly troublesome as there are non-standard ways in which millisecond jumps are represented in RINEX observation files (Guo and Zhang 2012). Some scholars suggested treating clock jumps as cycle slips or neglecting its effects within certain precision ranges for relative positioning. But for undifferenced processing, it may pose adverse effects on the PPP solution and result in repeated re-initialization or even non-convergence of the positioning results. Therefore, the first step of pre-processing for PPP should be devoted to compensating for receiver clock jumps.

We address issues related to receiver clock jump and its influence on PPP. In the first section, we define clock jumps and categorize them into four types according to their influence on GNSS observables. Afterwards, the consistency of observables affected by various types of clock jump is investigated, and a simple but rigorous approach for real-time clock jump compensation is proposed. Furthermore, the method is validated using more than 380 stations configured with about 35 different types of geodetic receivers. Finally, the contribution and performance of clock jump compensation to PPP are assessed.

Four types of clock jump presented in RINEX

Time tag (epoch value), pseudorange, and carrier phase are three fundamental RINEX quantities in a GPS observation file. Once the receiver clock bias exceeds a fixed threshold value, the clock reset mechanism adds an abrupt jump to the quantities. Due to the various steering mechanisms and reset options adopted by different manufactures and converter software, clock jumps may be presented in different forms.

Table 1 Four types of clock jump

Type	Time tag	Pseudorange	Carrier phase
1	Jumpy	Smooth	Smooth
2	Jumpy	Jumpy	Smooth
3	Smooth	Jumpy	Smooth
4	Smooth	Jumpy	Jumpy

Phenomenon of receiver clock jump

Four types of clock jump are defined in Table 1 according to its influence on the three fundamental quantities recorded by RINEX observation files.

Figure 1 presents a few examples of the above mentioned four types of clock jump. Each shows the behavior of time tag slip (Slip), pseudorange (C1), carrier phase (L1), and receiver clock bias (Bias), which can be derived by standard point positioning (SPP). The time tag slip (being jumpy) means an uneven data sampling according to the receiver time scale, which can be easily determined by differencing the predefined sampling interval and the actual interval of adjacent epochs.

As shown in Fig. 1a, the appearances of type 2 clock jumps are always accompanied with type 1 jumps. When the clock bias exceeds a predefined limit, a jump of an integer number of milliseconds is imposed only on the time tags (time tag slip) for type 1 clock jumps, leading to uneven data sampling but smoothly running receiver clock bias. The type 2 clock jump occurs periodically (every hour); both the time tag and pseudorange are reset simultaneously with the accumulated number of milliseconds. In Fig. 1b, c, two cases of type 3 clock jumps were shown with the same receiver type (SEPT POLARX2) but different jump values. As to the former one, once the receiver clock bias exceeds -0.5 ms, a distinct value of 1 ms is introduced to the pseudorange while the latter one jumps 19 ms as soon as the receiver clock bias exceeds -10 ms. As illustrated by Fig. 1d, type 4 clock jumps generate a synchronized discontinuity on pseudorange and carrier phase, both of which have a sawtooth clock signature; but the given time tags are kept as they are.

It should be noted that the clock adjustment is not always $+1$ or -1 ms; sometimes it may reach 19 ms per time. Even the same type of receiver may experience different types of clock jump, and the magnitude and frequency of clock jump varies from one to another. This mainly depends on the stability of the receivers' internal clock, the receiver manufacturers' clock drift management, and converter software we used.

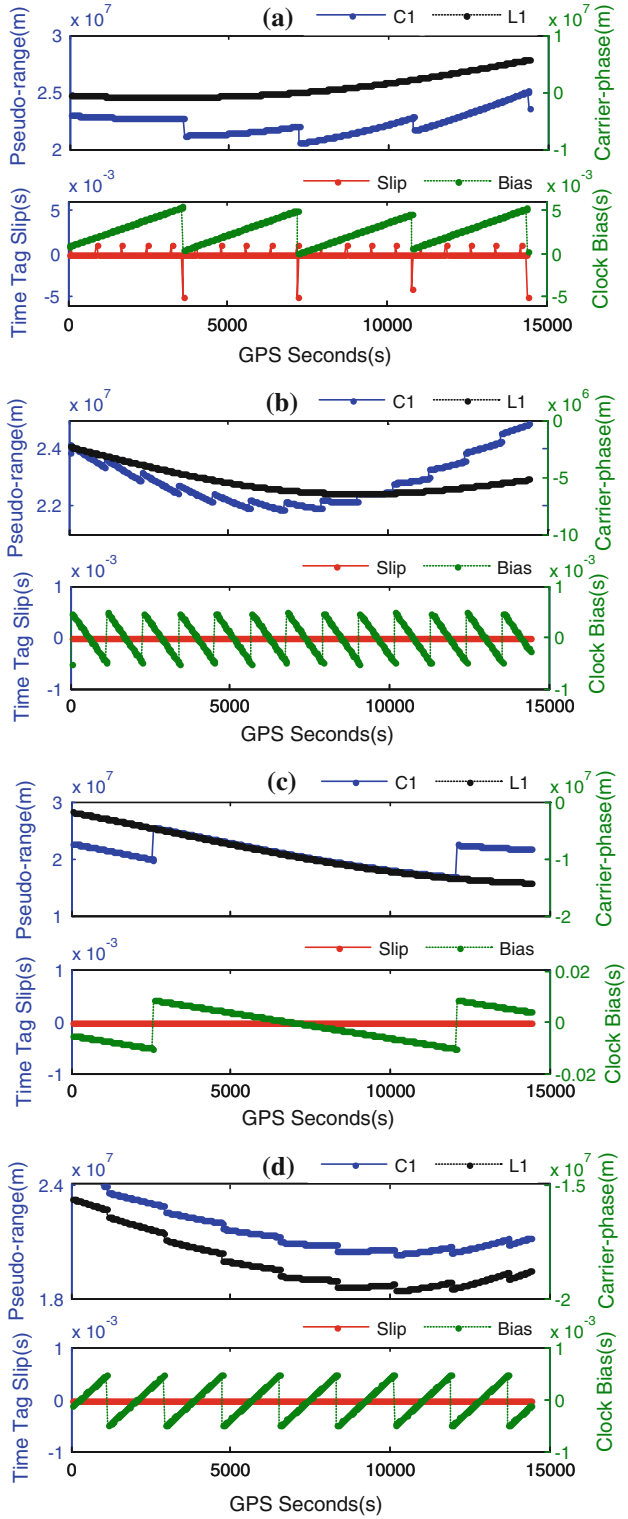

◀ **Fig. 1** Examples of the four types of clock jump. **a** A case of types 1 and 2 clock jump, recorded by a TRIMBLE 4000SSI receiver. The appearances of type 2 clock jumps are always accompanied with type 1 jumps; **b** a case of type 3 clock jump, recorded by a SEPT POLARX2 receiver. The value of receiver clock jump is always +1 ms; **c** another case of type 3 clock jump, recorded by a SEPT POLARX2 receiver. But the receiver clock jumps 19 ms per time; **d** a case of type 4 clock jump, recorded by a JPS LEGACY receiver. The value of receiver clock jump is always −1 ms

Observable consistency of various types of clock jump

Like cycle slips, clock jumps can lead to inconsistency in the GPS quantities, but there are essential differences between each. Cycle slips are discontinuities of an integer number of cycles in the carrier phase measurements resulting from temporary loss of lock in the carrier phase tracking loop, whereas clock jumps are discrete or continuous jumps introduced by receiver manufacturers to limit the magnitude of the clock offsets. Given a certain receiver clock reading and assuming a certain receiver clock jump, δ, the phase will, therefore, show two differences with a phase measured with a perfectly synchronized receiver: (1) a contribution from the incorrect reference frequency. Its size is $c^*\delta$ (in meters, c being the speed of light in vacuum); (2) another contribution from the dynamics of the satellite receiver system because the measurements have been performed too late (or early), approximately δ * beat frequency * λ (in meters, λ being the carrier wavelength). The pseudorange will also show exactly the same two items, with the "dynamic part" as well as $c^*\delta$. The former contribution cancels as soon as we are forming differences between observations of different satellites, while the latter one cannot be eliminated and should be carefully handled.

To generate a consistent set of observables, the following three different possibilities may be applied (Gurtner 2008): (1) we interpret the given epoch values as the readings of the original (i.e., non reset) receiver clock. We then have to correct the given observations by $\Sigma\delta$ * beat frequency * λ, $\Sigma\delta$ being the (signed) accumulated number of 1 millisecond resetting of the receiver clock. Of course, this linear correction is only an approximation; (2) we correct the given epochs with the accumulated number of millisecond jumps. In this case, we do not have to correct the phases, and we have a smoothly running receiver clock; (3) we leave the epochs and observations as they are, that is, we allow for a discontinuous receiver clock. However, we have to correct the phases by $c^*\Sigma\delta$ to get a consistent set of observables on the zero or single difference level. It is concluded that types 1 and 4 jumps follow the second and third approach, respectively, according to the performance of various types of clock jump as shown in Table 1 and Fig. 1. The pseudorange and carrier phase of these two types of clock jump are consistent and show the same receiver oscillator. As to types 2 and 3 clock jumps, the raw measurements are inconsistent since the receiver clock reset only adjust pseudorange, leaving the carrier phases uncorrected.

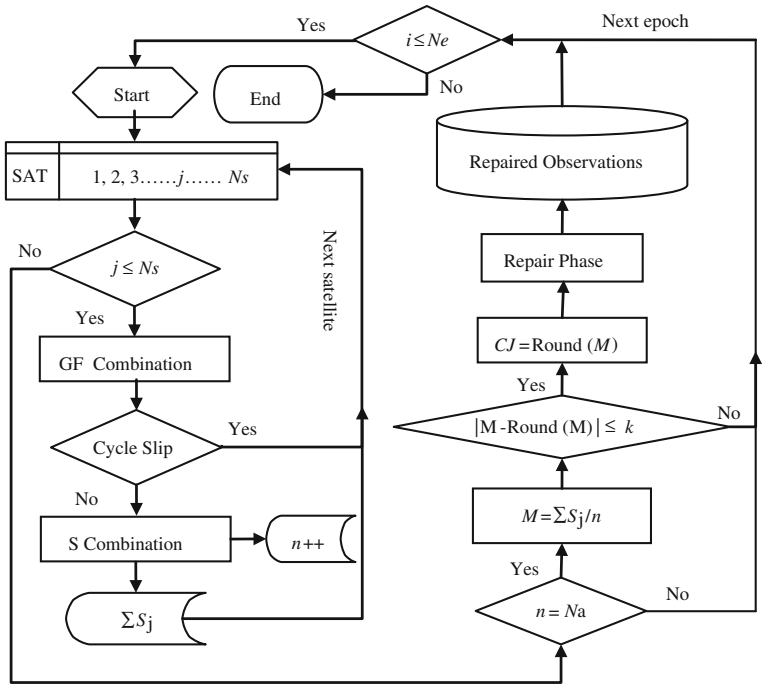

Fig. 2 Flow chart of the proposed real-time clock jump compensation method

Theoretically speaking, the inconsistency between pseudorange and carrier phase caused by clock jumps could be absorbed either by receiver clock bias or ambiguities, without affecting the coordinates (Krasner 1997). However, one should note that if we use a Kalman filter for data processing, as is often the case, care must be taken to properly detect and account for clock jumps prior to incorporating measurements into the filter, as without this data screening process, the filter will effectively see an error on all measurements.

Method of real-time clock jump compensation (RTCJC)

As presented in "Four types of clock jump presented in RINEX," the characteristics of clock jump are more or less known, and hence, it is possible to track and remove their effects. However, not all types of clock jump need correction. Only jumps of types 2 and 3 are of major concern and should be compensated to reconstruct a consistent set of observables. For simplicity, "clock jump" refers to types 2 or 3 clock jumps in the following text without any specific statement.

Most clock jumps can be easily captured either in the measurement or parameter domains. But clock jump detection based on the parameter domain is not a good choice for real-time data processing. Consequently, we propose a simple but rigorous methodology for clock jump compensation based on GNSS measurements. Figure 2 shows the procedure of clock jump detection and repair in detail. Since the algorithm requires only two adjacent data collection epochs (current epoch and previous epoch) for clock jump correction, it is suitable for real-time data processing.

Real-time clock jump detection

Like cycle slips, the effects of clock jump on GNSS measurements can be easily indentified due to their systematic characteristics. In this section, we first introduce an observable suitable for clock jump detection, and then, the discriminant criterion, threshold values, clock jump candidates, and validation procedures are illustrated in detail.

Clock jump observable

Suppose $\Delta P(i) = P(i) - P(i-1)$, $\Delta L(i) = L(i) - L(i-1)$, $i \ge 1$; and then, the clock jump detection observable S is constructed as follows

$$\begin{aligned} S^j(i) &= \Delta P^j(i) - \Delta L^j(i) \\ &= \Delta I_{i,i-1} - \lambda \cdot \Delta N_{i,i-1} + \Delta dP_{i,i-1} - \Delta dL_{i,i-1} + \xi, \end{aligned} \tag{1}$$

where the superscript "j" and subscript "i" represent a specific satellite and epoch; Δ is the epoch difference operator; I is the residual ionospheric delay; N is the ambiguity of the carrier phase; ΔdP and ΔdL are the offsets introduced by clock jump of the code (P) and carrier phase (L) measurements (in units of distance), respectively; λ is

the carrier wavelength; and ξ is the combination of residual error and noise.

As revealed in (1), the observable S is insensitive to receiver-satellite kinematics, and the non-dispersive delays are eliminated. All that is relevant is the residual ionospheric delay, cycle slip, clock jump, and measurement noise. Therefore, S is a good measure for detecting clock jumps if the effects of large cycle slips are excluded, and the residual ionospheric delay and noise are negligible.

To guarantee the reliability of the clock jump detection algorithm, we need another observable which is insensitive to clock jumps to eliminate the adverse effects of cycle slips during the detection. The Geometry-free (GF) combination

$$T_{\mathrm{GF}} = \Delta(L_1 - L_2) \tag{2}$$

can be used for this purpose (Blewitt 1990). Generally, once a clock jump occurs, the measurement of each frequency will experience an identical jump (in units of distance). Therefore, Eq. (2) will not be affected by clock jump during the cycle-slip-detection stage.

Discriminant criterion

Once a cycle slip is identified, observations of this satellite will be excluded from the subsequent clock jump detection. For satellites that have not been detected with cycle slip, Eq. (1) is used to calculate the clock jump detection observable. Excluding the effects of cycle slip, both the value of S and its rate of change are quite small and smooth when there are no clock jumps. When a clock jump occurs, a drastic change can be observed in S_j. Thus, the equation

$$\text{Jumps} = \begin{cases} 0, & |S_j| < k_1 \\ 1, & |S_j| \geq k_1 \end{cases} \tag{3}$$

can be utilized to preliminarily determine whether clock jumps occur for a specific satellite according to predefined threshold, where "0" means normal observation without any jump while "1" means possible clock jumps, and k_1 is the threshold value which will be specified in the following section.

Threshold values

Reasonable threshold value is critical for clock jump detection. In order to determine the values of k_1, we first analyze the time series of S with and without clock jumps. Figures 3 and 4 show the dual-frequency S ($S1$and $S2$) sequences corresponding to the satellite elevation at ALGO and ISTA stations, respectively. For this experimental data, there are no clock jumps at the ALGO station, while the receiver at ISTA has experienced three instances of 1-ms clock jumps during the observation period.

As shown in Figs. 3 and 4, without any clock jumps, the value of S is strongly correlated with the satellite elevation and ranges from a few decimeters to a few meters. This is due to the multipath effects and residual ionospheric delay. Hence, the ordinary noise of the S-combination is just at the meter level. Once a millisecond clock jump occurs, the S value will change dramatically reaching about 300 km for the G25 satellite at the ISTA site, which far exceeds the sum of multipath effects and residual ionospheric delay. Therefore, the S observable is quite sensitive to millisecond clock jumps.

The range error caused by 1 ms clock jump reaches $10^{-3} \cdot c$ (c means the speed of light in vacuum) meters. Taking into account the noise of the S-combination σ, threshold k_1 corresponding to the detection value $|S|$ can be given as follows

$$k_1 = 10^{-3} \cdot c - 3\sigma \tag{4}$$

in which typically $\sigma = 3$–5 m. Any jumps larger than or equal to 1 ms will be identified by this threshold.

Clock jump candidates and validation

As they are affected by the remaining gross errors and cycle slips, Eqs. (1) and (3) are not always effective in

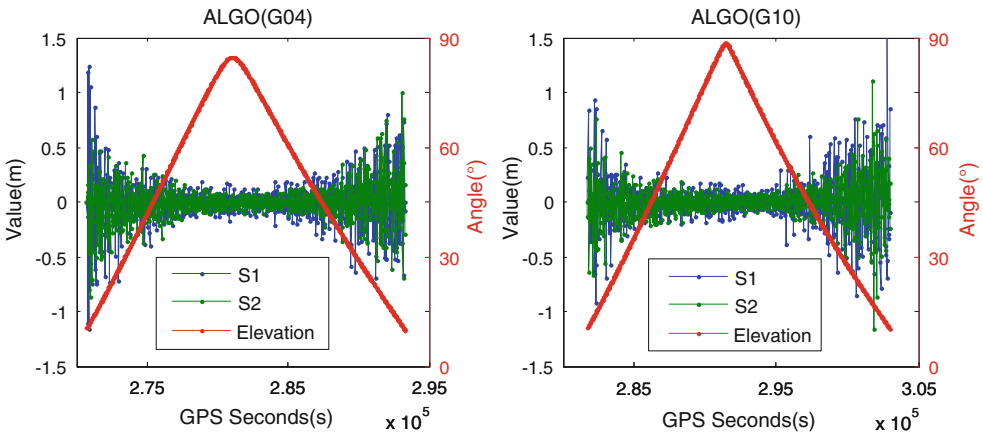

Fig. 3 Dual-frequency S sequences corresponding to satellite elevation at ALGO station. The *left one* shows the time series of $S1$, $S2$ for GPS PRN 04 satellite, and the *right one* shows the time series of $S1$, $S2$ for GPS PRN 10 satellite

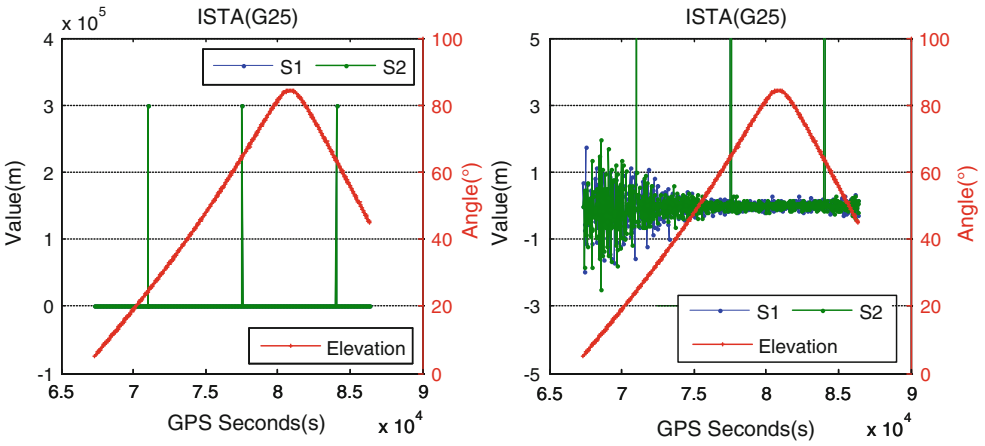

Fig. 4 Dual-frequency *S* sequences corresponding to satellite elevation at ISTA station. The *left one* shows the time series of *S1* and *S2* for GPS PRN 25 satellite. The *right one* is the amplification of the *graph* on the *left*, so as to clearly show the values of *S* when there is no clock jump

clock jump detection. Further confirmatory steps are necessary for validation. Due to the characteristic behavior of clock jumps, measurements from all the satellites and frequencies will simultaneously jump with a similar magnitude (in units of distance) when a clock jump occurs. This feature can be utilized to distinguish clock jumps from gross errors and cycle slips. Preliminary confirmation of a clock jump can be made by monitoring the number of affected satellites. If it is a clock jump, it should satisfy (5) for a specific epoch

$$n = \mathrm{Na},\ \mathrm{Na} \le \mathrm{Ns}, \tag{5}$$

where Ns is the total number of available satellites in the current epoch; Na is the number of valid satellites involved in clock jump detection, and n is the number of satellites flagged with possible millisecond clock jump. Since the satellites with gross errors or cycle slips are excluded from clock jump detection, Na is always smaller than or equal to Ns. Any event that satisfies (5) are considered to be either a clock jump or else a simultaneous large cycle slips on all satellites. Fortunately, the integer nature of millisecond clock jumps can be exploited to distinguish clock jumps from common cycle slips. Equation (6) can be further used to filter out the common cycle slip which generally has a float value in time units, and finally, the actual magnitude of the clock jump Js is determined by

$$M = 10^3 \cdot \left(\sum_{j=1}^{n} S^j \right) / (n \cdot c) \tag{6}$$

$$\mathrm{Js} = \begin{cases} \mathrm{Round}(M), & |M - \mathrm{Round}(M)| \le k_2 \\ 0, & |M - \mathrm{Round}(M)| > k_2 \end{cases}, \tag{7}$$

where $|\cdot|$ is the Absolute operator, Round is the Rounding Function. To determine the threshold k_2, Eq. (6) can be expanded as

$$\begin{aligned} M &= 10^3 \cdot \left(\sum_{j=1}^{n} S^j \right) / (n \cdot c) \\ &= \underbrace{10^3 \cdot \left(\sum_{j=1}^{n} \Delta \mathrm{d}P^j \right) / (n \cdot c)}_{\text{integer part}} + \underbrace{10^3 \cdot \left(\sum_{j=1}^{n} (\Delta I + \xi)^j \right) / (n \cdot c)}_{\text{fractional part}} \end{aligned} \tag{8}$$

in which the first part means the actual effect of millisecond jumps with an integer number, and the second part means the effect of residual errors with a fractional number. For a given residual error, such as 5–10 m, the fractional part is about $(2\text{–}3)\cdot 10^{-5}$ ms. Therefore, the threshold k_2 can be set to 10^{-4}–10^{-5} ms.

Real-time clock jump repair

Unlike cycle slip correction, clock jump repair is not the case of fixing discontinuities to keep the observations successive, since it may result in the cumulative increase of receiver clock bias, which goes against the objective of clock jump. As described in "Observable consistency of various types of clock jump," there are at least three different correction methods. We adopt the last approach, which is simple and has the advantage to not use any approximations or difficult interpolations. In other words, once a clock jump occurs, only the carrier phase measurements are adjusted to keep them consistent with code measurements. The repair formula can be expressed as

$$\widetilde{L}^j(i) = L^j(i) + \kappa \cdot Js \cdot c, \tag{9}$$

where L and $\widetilde{L}$ are the original and corrected carrier phase measurements, respectively; κ is a constant factor; for millisecond clock jumps, with $\kappa = 10^{-3}$.

Thanks to the integer nature of millisecond jump, we can easily fix and repair the clock jumps with a high confidence. As a matter of fact, clock jumps of types 2 and

Table 2 Results of clock jump detection

Site ID	Receiver type	Jump type	∑Js (ms)	Data source and length
ISTA	ASHTECH Z-XII3	3	13	IGS/24 h
METS	ASHTECH Z-XII3	1 and 2	37	IGS/05 h
BIS2	SEPT POLARX2	3	57	IGS/24 h
JASK	SEPT POLARX2	3	77	IGS/24 h
JOGJ	SEPT POLARX2	3	114	IGS/24 h
MARN	SEPT POLARX2	3	41	IGS/24 h
UNSA	SEPT POLARX2	3	76	IGS/24 h
ZWE2	SEPT POLARX2	3	57	IGS/24 h
GENO	TRIMBLE 4000SSI	1 and 2	−107	IGS/24 h
CAGL	TRIMBLE 4700	1 and 2	−52	IGS/24 h
MIKL	TRIMBLE 4700	1 and 2	−24	IGS/24 h
POLV	TRIMBLE 4700	1 and 2	38	IGS/24 h
SULP	TRIMBLE 4700	1 and 2	−21	IGS/24 h
INEG	TRIMBLE 5700	1 and 2	53	IGS/24 h
SMST	TRIMBLE 5700	1 and 2	78	IGS/24 h

3 are transformed into either types 1 or 4 clock jumps after being compensated by (9).

Data analysis on RTCJC

Dual-frequency GPS data from 384 IGS stations observed during day 100 in 2011 are used to illustrate the performance of our approach. The experimental data has involved 35 types of receivers, covering almost all the geodetic GNSS receivers commonly used at present.

Results of clock jump detection

About 5 different types of receiver located at 15 stations from the IGS permanent network have been detected as ms-level clock jumps (types 2 or 3). Table 2 shows the detection results including receiver type, jump type, and accumulative jump value ($\sum$**Js**).

Generally, the type of clock jump primarily depends on the clock steering management technique employed by the receiver's manufacturer. For instance, SEPT POLARX2 receivers usually present type 3 jumps, while TRIMBLE receivers always exhibit types 1 and 2 jumps. However, the data recorded by ASHTECH Z-XII3 receivers show three different types of clock jump. The accumulation of jumps depends on the stability of receiver clock. For example, due to long-term use and serious aging problems, the receiver clocks of GENO and JOGJ stations jump more than 100 ms during 24 h.

Determination of clock jump repair value

Like cycle-slip correction (Liu 2011), once a clock jump occurs, all the subsequent epochs should be repaired to take it into account. Figure 5 shows the instantaneous repair value (Rep) corresponding to the detection value (Det) of ms-level clock jumps at UNSA and CAGL stations.

As shown in Fig. 5, the clock jump detection value of UNSA is either 0 or 19 ms, and the detection value of CAGL is either 0 or −2 to −4 ms. The repair value gradually accumulates with the increase of clock jump frequency and value, and manifest as a step function. Before a new clock jump occurs, this repair value is a fixed integer; once a new clock reset occurs, the value of slip will be added to the current repair value and used as the new repair value for clock jumps at the subsequent epochs. During a single day, the accumulative repair value of UNSA and CAGL reaches to 77 and −53 ms, respectively.

PPP performances with and without RTCJC

To verify the performance of our approach, we have tested a large quantity of real data (as described in "Results of clock jump detection") with clock jumps in both static and kinematic modes, with and without RTCJC, using the Precise Point Positioning software—TriP developed by Wuhan University (Zhang and Andersen 2006). A Kalman Filter was utilized and the cutoff of satellites elevation was set as 5 degrees. Products such as precise satellite orbit, clock bias, and differential code bias (DCB) required for PPP were provided by the community of International

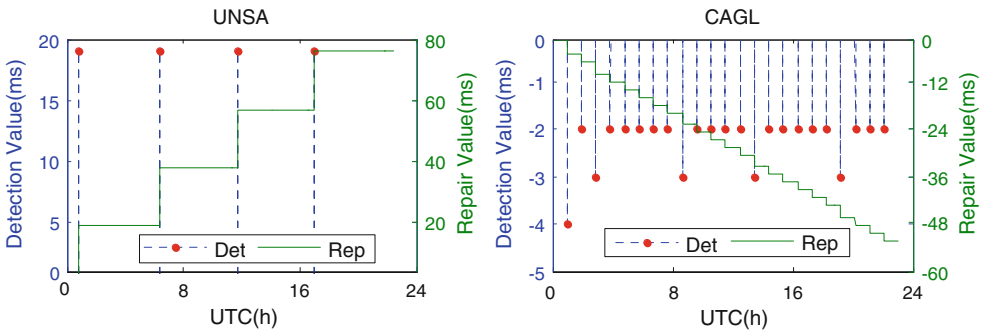

Fig. 5 Instaneous clock jump detection value (*Det*) and repair value (*Rep*). The *horizontal axis* indicates *UTC* time; the main *vertical axis* indicates *Det*, while the auxiliary *vertical axis* indicates *Rep*. The *left one* shows the time series of Det and Rep at UNSA station, and the *right one* shows the time series of Det and Rep at CAGL station

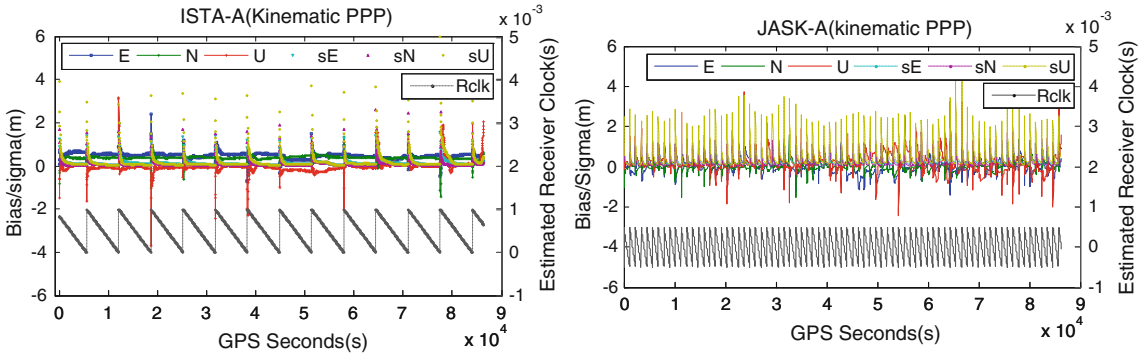

Fig. 6 Kinematic PPP results of *ISTA*/*JASK* without *RTCJC*. The *left one* shows the kinematic positioning error (*E/N/U*), standard deviation of coordinates (*sE/sN/sU*), and estimated receiver clock bias (*Rclk*) of *ISTA* station, and the right one shows the corresponding results of *JASK* once *RTCJC* is not applied

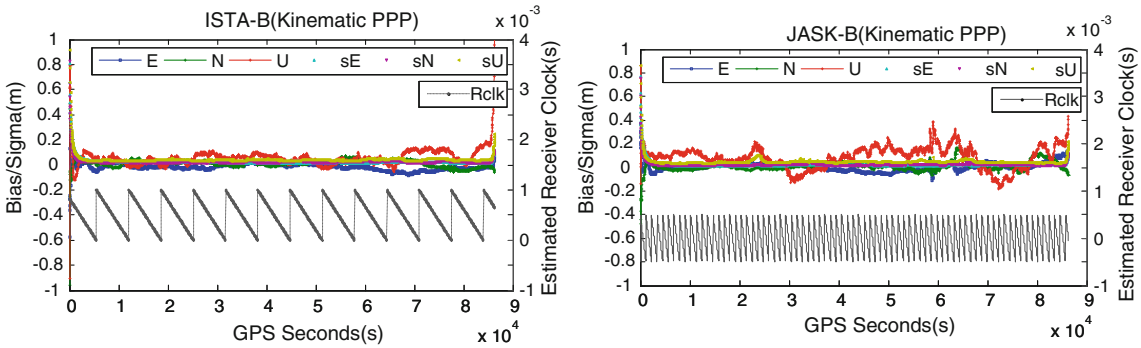

Fig. 7 Kinematic PPP results of *ISTA*/*JASK* with *RTCJC*. The *left one* shows the kinematic positioning error, standard deviation of coordinate, and estimated receiver clock bias of *ISTA* station, and the right one shows the corresponding results of *JASK* once *RTCJC* is applied

GNSS Service (Kouba and Heroux 2001; Bisnath and Gao 2007; Geng et al. 2010). Due to space limitation, only a few typical examples are present and analyzed in this section.

Kinematic PPP results

Figures 6 and 7 show the time series of kinematic positioning error and receiver clock bias processed with or without clock jump compensation on ISTA/JASK station. As illustrated in Fig. 6, it reveals that the positioning accuracy is quite sensitive to clock jumps if RTCJC procedures are not applied. Once a clock jump happens, the positioning accuracy dramatically decreases, and the bias reaches a few meters. This is reasonable when we acknowledge the fact that receiver coordinates are estimated as time-varying parameters in the kinematic PPP filter. And this poor performance can be attributed to the disruption of the cycle-slip detection process by clock jump, in which case all satellites would be erroneously assumed to have cycle slips. Consequently, the periodical clock jumps result in repeated re-initialization of the kinematic PPP solution, and the re-convergence on ISTA is possible around 30 min after a clock jump owing to the long interval between adjacent jumps (∼90 min). However, the frequent clock jumps with a short interval between each (∼18 min) on JASK are prone to cause the failure of re-convergence, and seriously affect the accuracy and efficiency of kinematic PPP. It seems unable to obtain a stable and accurate result. After a proper handling of jumps with RTCJC, as shown in Fig. 7, the positioning results are immune to clock jumps, which avoid a large number of unnecessary re-initializations. In addition, the convergence speed has obviously increased, and the positioning accuracy has been greatly improved as well.

Static PPP results

Likewise, the same data sets (ISTA and JASK) were used for static PPP solution with and without RTCJC, respectively, and the results are shown in Fig. 8. Similar but slightly different from Figs. 6 and 7, only solutions of the first 4 h are given to get a better show of the initialization.

As illustrated in Fig. 8, the accuracies of static PPP with and without RTCJC on ISTA are almost the same, and the effects of the clock jumps are negligible. The main reason is that, in static PPP mode, receiver coordinates are regarded as time-invariant parameters (process noise is set as 0). Even when a clock jump occurred without being

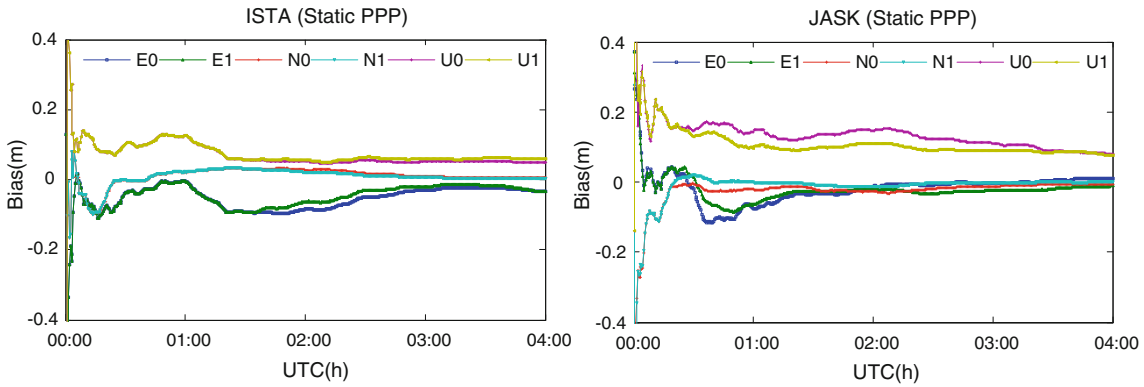

Fig. 8 Static PPP results of *ISTA*/*JASK*. The *left one* shows the static positioning error without *RTCJC* (*E0/N0/U0*) and the positioning error with *RTCJC* (*E1/N1/U1*) at *ISTA* station. The *right one* shows the corresponding error of *JASK* station

repaired, coordinate parameters can be effectively transferred through the state transition matrix in the kalman filter. Particularly after initialization, the accuracy of static PPP can be guaranteed by the tightly constrained state equations. However, when extremely frequent clock jumps occurred during the initialization stage (which generally takes 30 min or so) of static PPP at JASK station; it will result in over-dependence of filtering on the state equation and reduce the contribution of observations, which will certainly affect the convergence speed and accuracy of PPP. Once RTCJC is applied, higher precision observations can be fully taken advantage of and so result in a significant improvement in precision.

Therefore, to obtain an accurate and reliable solution, considerable attention should be paid to these clock jumps, and the RTCJC is necessary which has been confirmed to be effective.

Conclusions

We first provide a comprehensive classification of clock jumps according to their impact on GPS observations. To prevent the adverse effects of clock jumps, a simple but robust method of real-time clock jump compensation is proposed. Tests carried out in both static and kinematic modes have confirmed that our approach produces high performance. The following conclusions can be drawn from the study presented:

1. Owing to different clock steering mechanisms, clock jumps can be presented mainly in four categories according to their influence on GPS quantities. It should be noted that the clock adjustment is not always $+1$ or -1 ms. Sometimes, it may reach 19 ms per time. Even the same type of receiver may experience different types of clock jump, and the magnitude and frequency of clock jump varies from one to another. This mainly depends on the stability of the receivers' internal clock, the receiver manufacturers' clock drift management and software we used.
2. Although clock jump can lead to a discontinuity in the quantities of GPS data, not all types of clock jump need correction. Only jumps of types 2 and 3 are our major concern and should be compensated to reconstruct a consistent set of observables.
3. By applying the proposed method, clock jumps presented in GPS data can be effectively identified and repaired accurately, and a large number of unnecessary re-initializations of the PPP will no longer be triggered by receiver clock jumps. This gives a significant improvement in PPP accuracy and reliability. Therefore, in order to ensure a continuous, accurate, and reliable solution, real-time clock jump detection and repair are necessary and important for PPP.

Acknowledgments The authors gratefully acknowledge IGS and CODE community for providing global GNSS data and products. We also appreciate two anonymous reviewers and the editor in chief for their valuable comments and improvements to this manuscript. This study was supported by the Founds for Innovative Research Group of the National Natural Science Foundation of China (Grant No. 41021061) and National Natural Science Foundation of China (Grant No. 41074024).

References

Bisnath S, Gao Y (2007) Current state of precise point positioning and future prospects and limitations. In: Sideris MG (ed) Observing our changing Earth. Springer, New York, pp 615–623

Blewitt G (1990) An automated editing algorithm for GPS data. Geophys Res Lett 17(3):199–202

Estey LH, Meetens CM (1999) TEQC: the multi-purpose toolkit for GPS/GLONASS data. GPS Solut 3(1):42–49. doi:10.1007/PL00012778

Freymueller JT (2003) IGSMAIL-4318: new version of ClockPrep program. IGS central bureau

Geng JH, Teferle FN, Meng X, Dodson AH (2010) Kinematic precise point positioning at remote marine platforms. GPS Solut 14(4):343–350. doi:10.1007/s10291-009-0157-9

Guo F, Zhang XH (2012) Real-time clock jump detection and repair for precise point positioning. In: Proceedings of the ION GNSS 2012, 17–21 Sept, Nashville, USA

Gurtner WL (2008) The RINEX format: current status, future developments. In: Proceedings of IGS analysis center workshop 2008, 2–6 June, Miami, USA

Gurtner WL, Estey L (2007) RINEX: the receiver independent exchange format version 2.11. IGS Central Bureau

Kim D, Langley RB (2001) Instantaneous real-time cycle-slip correction of dual frequency GPS data. In: Proceedings of the international symposium on kinematic systems in geodesy, geomatics and navigation, 5–8 June, Banff, Alberta, Canada

Kim HS, Lee HK (2009) Compensation of time alignment error in heterogeneous GPS receivers. In: Proceedings of the 13th IAIN world congress, 27–30 Oct, Stockholm, Canada

Kouba J, Heroux P (2001) Precise point positioning using IGS orbit and clock products. GPS Solut 5(2):12–28. doi:10.1007/PL00012883

Krasner N (1997) GPS receiver and method for processing GPS signal. US Patent 5663734, 2 Sept 1997

Liu ZZ (2011) A new automated cycle slip detection and repair method for a single dual-frequency GPS receiver. J Geod 85(3):171–183. doi:10.1007/s00190-010-0426-y

Lonchay M, Bidaine B, Warnant R (2011) An efficient dual and triple frequency preprocessing method for GALILEO and GPS signals. In: Proceedings of the 3rd international colloquium-scientific and fundamentals aspects of the GALILEO programme, 31 Aug–2 Sept, Copenhagen, Denmark

Mireault Y, Tetreault P, Lahaye F, Collins P, Caissy M (2008) Real-time and near real-time GPS products and services from Canada. In: Proceedings of IGS analysis center workshop 2008, 2–6 June, Miami, USA

Zhang XH, Andersen OB (2006) Surface ice flow velocity and tide retrieval of the Amery ice shelf using precise point positioning. J Geod 80(4):171–176

Author Biographies

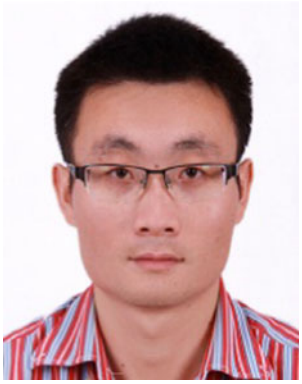

Fei Guo is currently a Ph.D. candidate at School of Geodesy and Geomatics, Wuhan University, China. He obtained his B.Sc. and M.Sc degrees in 2007 and 2009, respectively. His current research focuses mainly involve GNSS precise point positioning and quality control technology, etc.

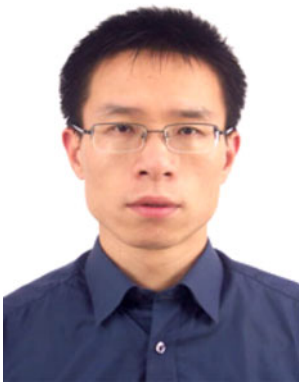

Xiaohong Zhang is currently a professor at the Wuhan University. He obtained his B.Sc., Master and Ph.D. degrees with distinction in Geodesy and Engineering Surveying at the School of Geodesy and Geomatics in Wuhan University in 1997, 1999, and 2002. His main research interests include precise point positioning (PPP) and GNSS/INS.